Supporting Information

Particle size and mixing state of freshly emitted black carbon from different combustion sources in China

Yuxuan Zhang[1], Qiang Zhang[1], Zhiliang Yao[3], and Haiyan Li[2]*

[1]Ministry of Education Key Laboratory for Earth System Modelling, Department of Earth System Science, Tsinghua University, Beijing 100084, People's Republic of China

[2]State Key Joint Laboratory of Environment Simulation and Pollution Control, School of Environment, Tsinghua University, Beijing 100084, People's Republic of China

[3]Department of Environmental Science and Engineering, Beijing Technology and Business University, Beijing 100048, People's Republic of China

[*]Correspondence author: qiangzhang@tsinghua.edu.cn

Table of content:

S1. Source measurement

We sampled smoke plumes close to the exhaust outlets for the emission sources of diesel vehicles (DV), brick kilns (BK), residential crop residue burnings (CR) and residential firewood burnings (FW) in September and October 2014 at North China Plain (NCP). Figure S1 shows the experimental setup. The distance between exhaust outlet and inlet of sampling tube was within 0.2 m and the sampling line was 2-3 m, correspondingly the transit time was 30-60 seconds. Each experiment lasted for 0.5-2 hours to sample freshly emitted BC particles. We performed on-road emission tests of diesel vehicles. The exhaust particles from the diesel test vehicles were collected and measured. The experiments of BK emission were conducted on the roof of kilns. For the CR and FW burnings in the stove of Chinese kang, the smoke went through a kang body and then a chimney and finally was sampled close to the chimney outlets.

The source emission measured in our study characterized the properties of the fresh smoke plumes that just emitted into atmosphere, which were affected by the processes of combustion and emission. In this study, the emission not only involves in the stage through the exhaust pipe/chimney, but also includes the process emitted into atmosphere from exhaust outlets. During the process emitted into atmosphere, the temperature and vapor pressure will sudden change, which may lead to change in BC properties (e.g., mixing state) due to interaction with co-emitted species. This change during emission process may different with that occurring during atmospheric transport. Generally, model studies only consider the change in BC mixing state during atmospheric transport. Therefore, the change during the process emitted into atmosphere should be included in the initial feature of source emission, as a "initializing point" to model the subsequent ageing of BC during atmospheric transport.

As the initial feature of source emission, the effect of background air on measurements should be excluded. In our measurement, we sampled close to the exhaust outlet and the residence time was within a minute. Previous studies[1-3] showed that the maximum of BC aging rate coefficient in China was about 20% h^{-1} (i.e., 0.3% min^{-1}). This indicated that the effect of background air on our measurements (i.e., particle size and mixing state) of emitted BC is little.

The four types of source emission measured in this study are representative in China. As a main source of BC emission in traffic sector, different kinds of diesel vehicles (i.e., light-duty and heavy-duty) under different conditions (idle speed and normal running on the highways and city roads) were sampled. The differences in the properties (mass averages of size and mixing state) of emitted BC particles among various samples are within 10%. The brick kilns, to some extent, can represent coal burning source. Our measurements on brick kilns (i.e., ~230 nm of MMD of BC core) were similar with those (i.e., ~215 nm of MMD) obtained from coal burning sources in China reported by Wang et al. (2016).[4] Crop residue and firewood are commonly used for cooking and heating in rural China, and therefore we chose them as a type of emission source (i.e., biofuel burning) in residential sector. In terms of CR and FW, the measurements show that there are wide range of particle size and mixing state of BC, which characterize the difference under different combustion and emission conditions. The results are comparable with measurements of biomass burning in the chamber reported by Pan et al. (2017).[5]

S2. SP2 Data Analysis

The size and mixing state of freshly emitted BC particles were retrieved by SP2 measurements. The data measured by SP2 are incandescence and scattering signals of a single BC-containing particle induced by a 1064 nm Nd:YAG intra-cavity laser. The SP2 data process and analysis included calibration, correction, LEO fitting, retrieval of refractive index of coating materials (RI_s), Mie calculation and sensitivity tests (uncertainty analysis).

The calibration of incandescence and scattering signals are needed to obtain the mass of refractory BC (rBC) and scattering cross section (C_s) of whole BC-containing particle (core+shell). In this study, we used Aquadag with DMA-SP2 system to calibrate the incandescence signals of SP2. The calibration curve was fitted by recording the incandescence signal peak heights for Aquadag particles of known masses[6]. The calibration using Aquadag particles is corrected based on the different sensitivity of SP2 to ambient rBC and Aquadag[7]. On the other hand, polystyrene latex spheres were used to calibrate the scattering signal, which is proportional to the C_s. We did the SP2 calibration two times, namely one before the measurement (at the end of September 2014) and another after the measurement (at the end of October 2014). The difference between two calibrations was lower than 3%, demonstrated the stability of our SP2 performance.

In order to address the limitation of SP2 measurements, they were corrected by detection efficiency curve and data fitting. The SP2 count efficiency was obtained by comparing with CPC count. Both CPC and SP2 were set up installed downstream of the DMA. Figure S2 shows the SP2 detection efficiency curve. It is noted that the SP2 detection efficiency curve used in this work (September-October 2014) was the same with that used in the ambient measurement on October-November in Beijing,[8, 9] taking into account the stability of our SP2 performance. The lower size limit is about ~70 nm for SP2 measurement. The size distribution was fitted by Gaussian function, and the size at fitted peak is taken as a median value.

The RI_s values of fresh BC particles from various emission sources are needed to retrieve D_p and absorption properties (i.e., MAC and E_{ab}) by Mie calculation. In this study, the real part of RI_s was determined by a closure study based on DMA-SP2 measurements[3]. Three hypotheses are made using this method: (1) the image part of RI_s is presumed to be 0, taking into account that scattering property (i.e.,

C_s) at a larger wavelength (i.e., 1064 nm) from SP2 measurements is used; (2) RI_s has a same value with the refractive index of non-BC particles ($RI_{non\text{-}BC}$), assuming that coating materials have the same chemical compositions as the non-BC particles; (3) for non-BC particle, the optical size is almost equal to its mobility size assuming their near-spherical shape. Based on these assumptions, we scanned different values of $RI_{non\text{-}BC}$ until the calculated optical diameter of non-BC particle based on SP2 measurements matches the selected mobility diameter by DMA. In terms of the imaginary part of RI_s, which can characterize the absorption by the coating materials, was presumed to be 0 for retrieval of D_p based on C_s at 1064 nm from SP2 measurements. When to calculate the light absorption of BC at an ultraviolet wavelength (i.e., 400 nm), we assumed a value of 0.005 according to literature[10].

We further did the sensitivity tests to evaluate the uncertainties in the determined size, mixing state and light absorption of BC particles caused by the uncertainties in RI_s. Figure S3a shows that the imaginary part of RI_s had little (<1% uncertainty) effect on retrieval of D_p, demonstrating a reasonable value of 0 used in retrieval of particle size of BC based on SP2 measurements. Figure S3b displays the dependence of D_p on the real part of RI_s. The D_p decrease with increase in the real part of RI_s. Considering that the values of real part of refractive index for non-BC components are mainly in the range of 1.4-1.7[11-14], the uncertainties in D_p caused by the uncertainties in RI_s for the four types of emission sources were estimated to be lower than 10%. The uncertainty in BC mixing state (i.e., D_p/D_c) was dominated by the uncertainty in D_p. In terms of E_{ab} at 400 nm, we determined their dependence on the imaginary part of RI_s in the range of 0-0.03 (Fig. S4), which were adopted based on report by Liu et al. (2015).[10] Figure S4 shows that E_{ab} at 400 nm increased with increasing in the imaginary part of RI_s in this range, with lower than 5% difference in this range for the four types of emission sources, indicating that the imaginary part of RI_s had a little effect to estimate the light absorption of fresh emitted BC from the sources investigated in this study, even at ultraviolet wavelength range.

S3. Comparison the measurements between two systems

The measurements of SP2 installed downstream of a dilution section (system 1) and a DMA (system 2) shown in Fig. S1 are compared. The concentration of collected particles from exhaust flow is too high for SP2 measurement. In order to lower the particle concentration before passing through SP2, a dilution system with a dilution rate in the range of 20:1 to 50:1 was installed upstream of the SP2. However, we could not know whether the BC mixing state would change during dilution. In order to answer this question, we set up DMA-SP2 system to compared with Dilution-SP2 measurement. The DMA with a sheath to sample flow ratio of 5:1 was used to selected size-resolved particles and then measured by SP2. The DMA-SP2 system can also achieve lower particle concentrations in SP2 measurement due to mono-dispersed selected by DMA. However, the Dilution-SP2 system measured poly-dispersed particles. Therefore, direct comparison between the measurements of the two systems was unreasonable.

In order to address this limitation, when doing the data process for the measurements of Dilution-SP2 systems, parts of ones were chosen to compare with DMA-SP2 measurements. Criteria for selecting data sets depended on the optical size rather than mobility size of BC-containing particles measured by DMA-SP2. According to the measurements from Dilution-SP2 system, we got that the CMD of DV, CR and FW combustion sources are ~182, ~359 and ~316 nm, respectively. In order to make the measurements from the two systems comparable, we only use one DMA-selected size data near CMD (i.e., 200, 400 and 300 nm for DV, CR and FW, respectively) to further compare the coating thickness of BC (Fig. S5) from the two systems. The median of optical size of BC-containing particles in DMA-SP2 measurements was determined by the peak position of size distribution (Fig. S5a), with values of 170, 433 and 349 nm for emission sources of DV, CR and FW, respectively. Based these optical sizes, the BC-containing particles in the Dilution-SP2 measurement with similar optical sizes (i.e., 170±10, 433±10 and 349±10 nm for emission sources of DV, CR and FW, respectively) were used as a data set for further statistics of their coating thickness, with medians of 29±3, 154±8 and 99±6 nm for emission sources of DV, CR and FW, respectively. They are comparable with the medians of coating thickness of BC-containing particles measured by DMA-SP2, namely, 27±2, 150±6 and 98±5 nm (Fig. S5c and 5d), revealing that a little change (lower than 5%) in BC coating materials during dilution for our source

emission measurements. This may be due to low volatility of coating materials formed during the initial aging stage (i.e., combustion and emission process) with high temperature, which are difficult to evaporate during dilution.

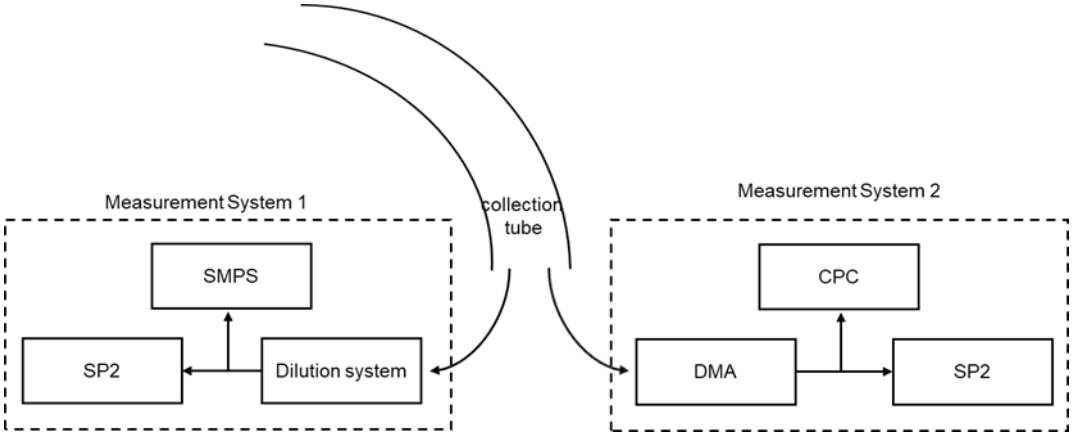

Figure S1. Schematic of the instrument setup.

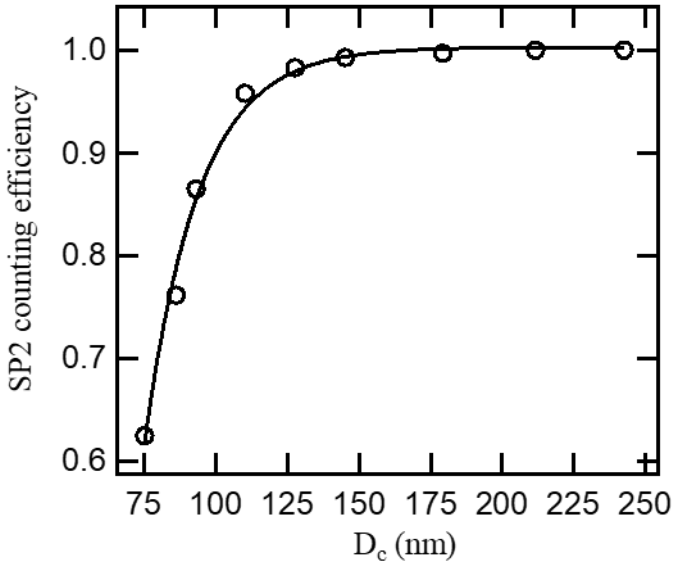

Figure S2. SP2 detection efficiency in each rBC size-bin.

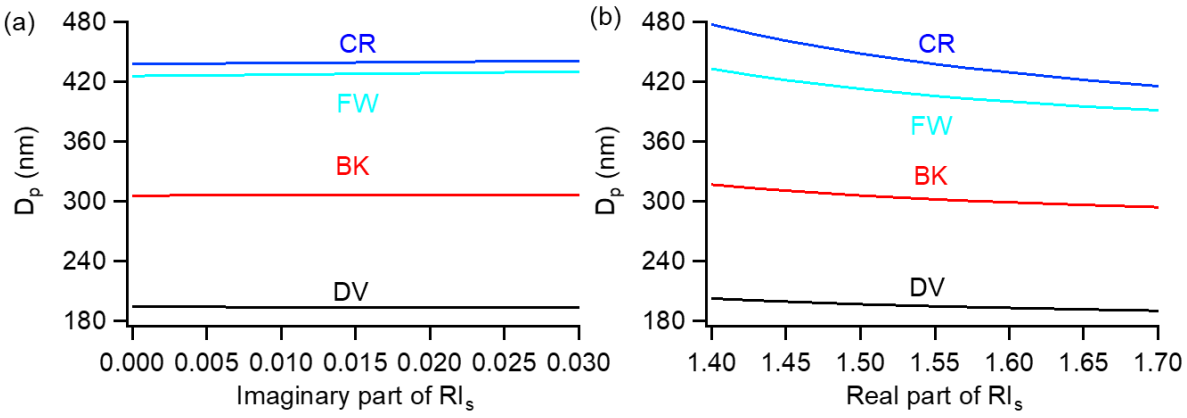

Figure S3. Dependence of retrieved D_p on (a) imaginary part and (b) real part of RI_s.

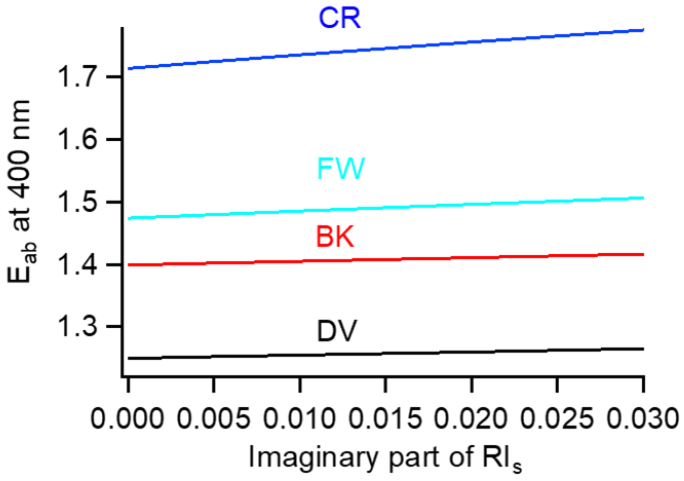

Figure S4. Dependence of calculated E_{ab} at 400 nm on imaginary part of RI_s.

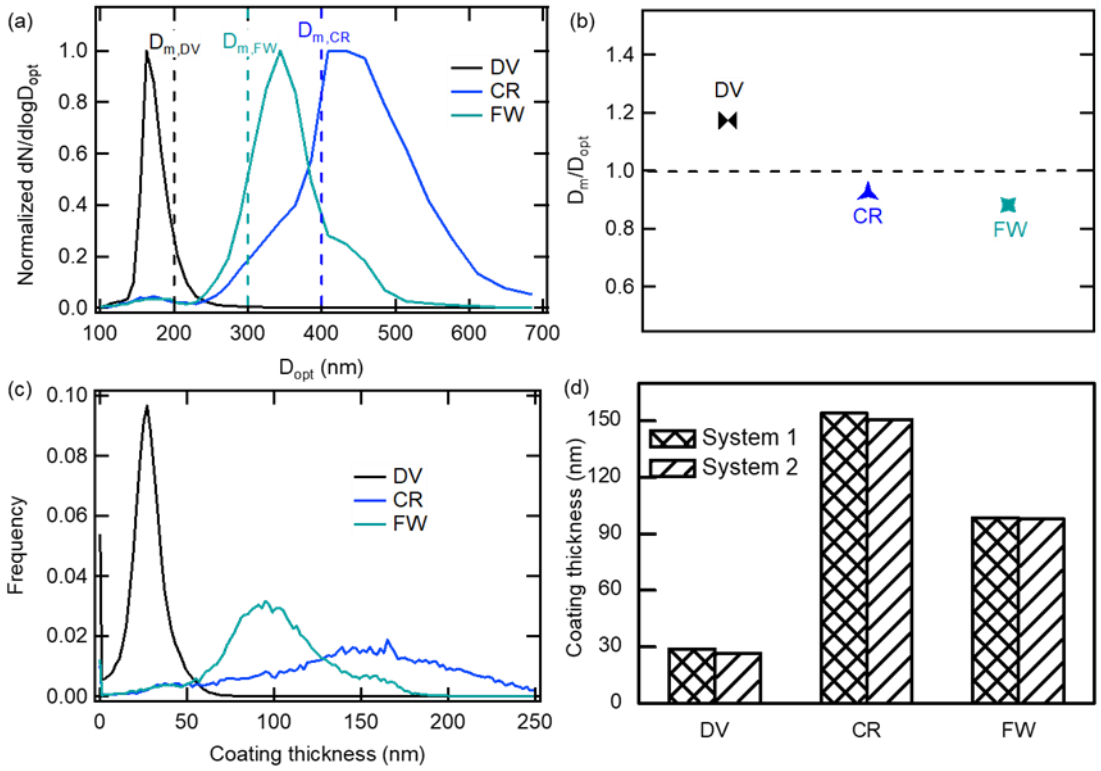

Figure S5. Particle size and mixing state of size-resolved BC from DMA-SP2 measurement. (a) Optical size (D_{opt}) distribution from SP2 measurement for size-resolved BC particles selected by DMA with mobility diameters (D_m) of 200, 400 and 300 nm (dash lines) for emission sources of DV, CR and FW, respectively. (b) The ratio of the selected D_m to the median D_{opt} (D_m/D_{opt}) for the BC-containing particles. (c) The frequency distribution of coating thickness of size-resolved BC particles. (d) Comparison of the median coating thickness of BC from the Dilution-SP2 (system 1) and DMA-SP2 (system 2) measurements.

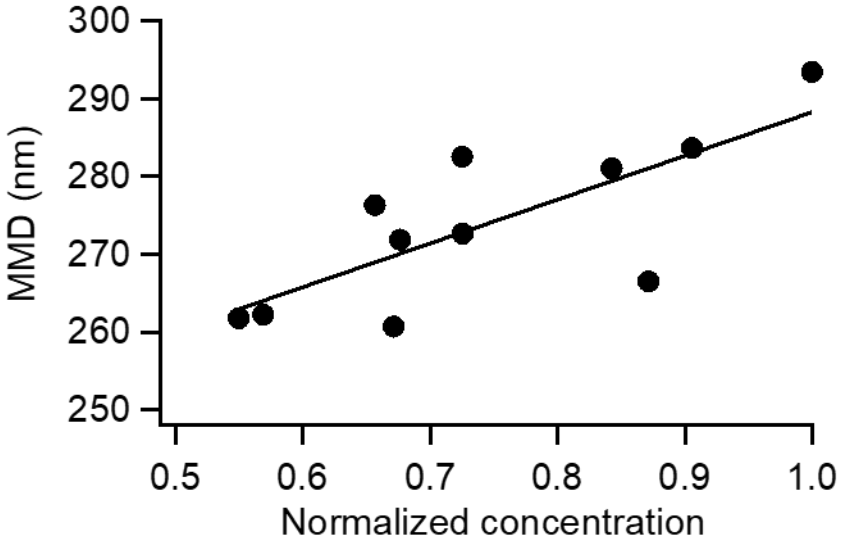

Figure S6. Correlation between core size and BC number concentration for FW source.

References

1. Cheng, Y. F.; Su, H.; Rose, D.; Gunthe, S. S.; Berghof, M.; Wehner, B.; Achtert, P.; Nowak, A.; Takegawa, N.; Kondo, Y.; Shiraiwa, M.; Gong, Y. G.; Shao, M.; Hu, M.; Zhu, T.; Zhang, Y. H.; Carmichael, G. R.; Wiedensohler, A.; Andreae, M. O.; Pöschl, U., Size-resolved measurement of the mixing state of soot in the megacity Beijing, China: diurnal cycle, aging and parameterization. *Atmos. Chem. Phys.* **2012,** *12*, (10), 4477-4491.

2. Zhang, Y.; Li, M.; Cheng, Y.; Geng, G.; Hong, C.; Li, H.; Li, X.; Tong, D.; Wu, N.; Zhang, X.; Zheng, B.; Zheng, Y.; Bo, Y.; Su, H.; Zhang, Q., Modeling the aging process of black carbon during atmospheric transport using a new approach: a case study in Beijing. *Atmos. Chem. Phys.* **2019,** *19*, (14), 9663-9680.

3. Zhang, Y.; Su, H.; Ma, N.; Li, G.; Kecorius, S.; Wang, Z.; Hu, M.; Zhu, T.; He, K.; Wiedensohler, A.; Zhang, Q.; Cheng, Y., Sizing of Ambient Particles From a Single-Particle Soot Photometer Measurement to Retrieve Mixing State of Black Carbon at a Regional Site of the North China Plain. *Journal of Geophysical Research: Atmospheres* **2018,** *123*, (22), 12778-12795.

4. Wang, Q.; Huang, R.-J.; Zhao, Z.; Cao, J.; Ni, H.; Tie, X.; Zhao, S.; Su, X.; Han, Y.; Shen, Z.; Wang, Y.; Zhang, N.; Zhou, Y.; Corbin, J. C., Physicochemical characteristics of black carbon aerosol and its radiative impact in a polluted urban area of China. *Journal of Geophysical Research: Atmospheres* **2016,** *121*, (20), 12505-12519.

5. Pan, X.; Kanaya, Y.; Taketani, F.; Miyakawa, T.; Inomata, S.; Komazaki, Y.; Tanimoto, H.; Wang, Z.; Uno, I.; Wang, Z., Emission characteristics of refractory black carbon aerosols from fresh biomass burning: a perspective from laboratory experiments. *Atmos. Chem. Phys.* **2017,** *17*, (21), 13001-13016.

6. Gysel, M.; Laborde, M.; Olfert, J. S.; Subramanian, R.; Gröhn, A. J., Effective density of Aquadag and fullerene soot black carbon reference materials used for SP2 calibration. *Atmos. Meas. Tech.* **2011,** *4*, (12), 2851-2858.

7. Laborde, M.; Mertes, P.; Zieger, P.; Dommen, J.; Baltensperger, U.; Gysel, M., Sensitivity of the Single Particle Soot Photometer to different black carbon types. *Atmos. Meas. Tech.* **2012,** *5*, (5), 1031-1043.

8. Zhang, Y.; Li, X.; Li, M.; Zheng, Y.; Geng, G.; Hong, C.; Li, H.; Tong, D.; Zhang, X.; Cheng, Y.; Su, H.; He, K.; Zhang, Q., Reduction in black carbon light absorption due to multi-pollutant emission control during APEC China 2014. *Atmos. Chem. Phys.* **2018,** *18*, (14), 10275-10287.

9. Zhang, Y.; Zhang, Q.; Cheng, Y.; Su, H.; Li, H.; Li, M.; Zhang, X.; Ding, A.; He, K., Amplification of light absorption of black carbon associated with air pollution. *Atmos. Chem. Phys.* **2018,** *18*, (13), 9879-9896.

10. Liu, S.; Aiken, A. C.; Gorkowski, K.; Dubey, M. K.; Cappa, C. D.; Williams, L. R.; Herndon, S. C.; Massoli, P.; Fortner, E. C.; Chhabra, P. S.; Brooks, W. A.; Onasch, T. B.; Jayne, J. T.; Worsnop, D. R.; China, S.; Sharma, N.; Mazzoleni, C.; Xu, L.; Ng, N. L.; Liu, D.; Allan, J. D.; Lee, J. D.; Fleming, Z. L.; Mohr, C.; Zotter, P.; Szidat, S.; Prévôt, A. S. H., Enhanced light absorption by mixed source black and brown carbon particles in UK winter. *Nature Communications* **2015,** *6*, 8435.

11. He, Q.; Bluvshtein, N.; Segev, L.; Meidan, D.; Flores, J. M.; Brown, S. S.; Brune, W.; Rudich, Y., Evolution of the Complex Refractive Index of Secondary Organic Aerosols during Atmospheric Aging. *Environmental Science & Technology* **2018,** *52*, (6), 3456-3465.

12. Liu, P. F.; Abdelmalki, N.; Hung, H.-M.; Wang, Y.; Brune, W. H.; Martin, S. T., Ultraviolet and visible complex refractive indices of secondary organic material produced by photooxidation of the aromatic compounds toluene and *m*-xylene. *Atmos. Chem. Phys.* **2015,** *15,* 1435–1446.

13. Nakayama, T.; Sato, K.; Matsumi, Y.; Imamura, T.; Yamazaki, A.; Uchiyama, A., Wavelength and NO_x dependent complex refractive index of SOAs generated from the photooxidation of toluene. *Atmos. Chem. Phys.* **2013,** *13*, (2), 531-545.

14. Flores, J. M.; Zhao, D. F.; Segev, L.; Schlag, P.; Kiendler-Scharr, A.; Fuchs, H.; Watne, Å. K.; Bluvshtein, N.; Mentel, T. F.; Hallquist, M.; Rudich, Y., Evolution of the complex refractive index in the

UV spectral region in ageing secondary organic aerosol. *Atmospheric Chemistry & Physics* **2014,** *14*, (3) 5793-5806.